RESEARCH ARTICLE SUMMARY

TISSUE REGENERATION

URI is required to maintain intestinal architecture during ionizing radiation

Almudena Chaves-Pérez, Mahmut Yilmaz*, Cristian Perna*, Sergio de la Rosa, Nabil Djouder†

INTRODUCTION: Exposure to high-dose irradiation (>10 gray) from the uncontrolled release of radioactive materials or intensive radiotherapy for cancer treatment can cause gastrointestinal syndrome (GIS), a lethal disorder affecting the intestinal structure. Symptoms and signs include nausea, diarrhea, vomiting, bleeding, and intestinal perforation, leading to the death of the patient through bacterial infection and septic shock. Treatments are very limited and generally focused on reducing GIS symptoms. Natural products, dietary interventions, and antioxidants have also been tested preclinically but have shown very modest effects in mitigating GIS. To assess medical countermeasures, it is essential to develop specific and robust animal models in which the relationship between radiation doses, GIS incidence, and severity can be correlated with the histopathology of the intestine. Here, we aim to understand cell biology and molecular events of GIS after radiation exposure by using a genetic GIS mouse model generated in our laboratory. This information will help in identifying biomarkers that can predict degrees of intestinal toxicity after severe ionizing radiation and assist in developing procedures to protect against GIS.

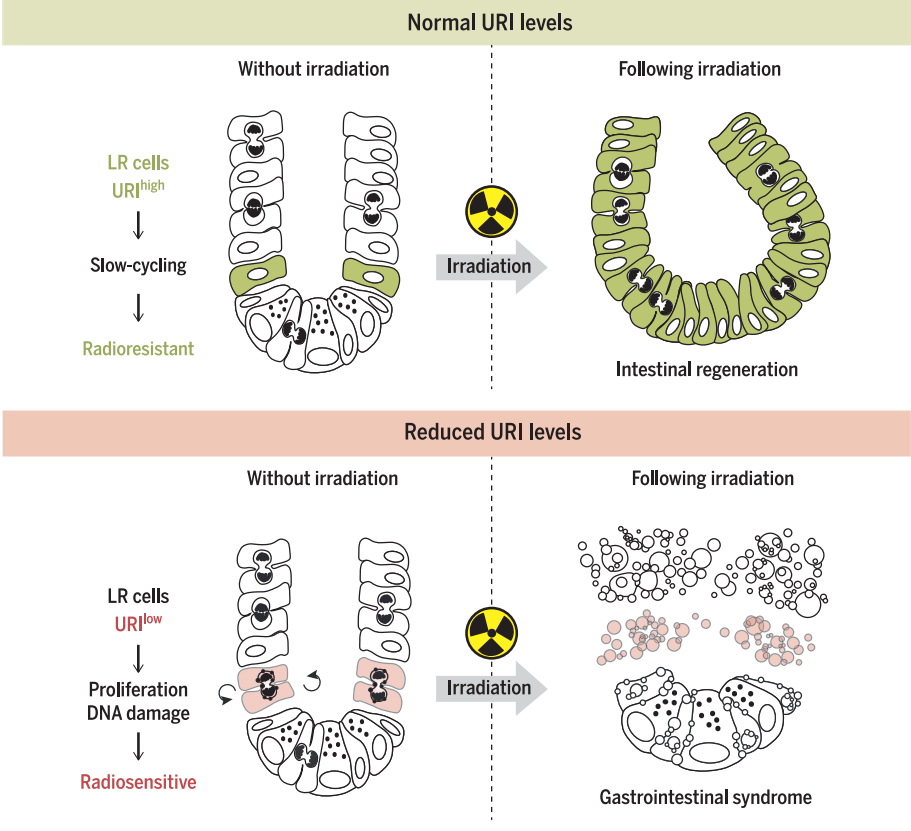

Schematic summarizing the role of URI in GIS. (Top) URI is a marker of the slow-cycling LR cells. URI-positive (URI^{high}) slow-cycling cells are radioresistant. URI^{high} slow-cycling cells within the crypts represent the facultative stem cell pool essential for organ regeneration after high-dose irradiation. (Bottom) Reduced URI levels (URI^{low}) increase proliferation and DNA damage in LR cells, rendering them radiosensitive.

RATIONALE: High levels of DNA damage and cell death are well-known clinical features of intestinal radiation toxicity. The molecular chaperone unconventional prefoldin RPB5 interactor (URI) reportedly controls and protects genome integrity in response to environmental insults. Therefore, we hypothesized that URI may play an important role in ensuring genome stability in the highly proliferative intestinal epithelium after exposure to ionizing radiation. By using genetically engineered mouse models for URI gain- and loss-of-function specifically in the intestinal epithelium, we studied the role of URI in GIS.

ON OUR WEBSITE

Read the full article at http://dx.doi.org/10.1126/science.aaq1165

RESULTS: URI levels fluctuate in intestinal crypts dose- and time-dependently after different doses of ionizing radiation. Specifically, URI increases at early postirradiation stages (24 to 48 hours), correlating with activation of the DNA damage response, whereas URI levels decrease during the regenerative response (72 to 96 hours postirradiation). We altered the level of URI and found that overexpression in mouse intestinal epithelium protects against intensive ionizing radiation and GIS, whereas halving URI expression sensitizes to ionizing radiation. Moreover, genetic URI ablation in the intestine caused mouse death, mimicking features of human GIS. We show that URI labels the slow-dividing stem cell–like label-retaining (LR) cells and is essential for protecting them from death, allowing the regeneration of the injured organ after high-dose irradiation. Mechanistically, we demonstrate that URI loss activates the β–catenin–c-MYC axis specifically in LR cells. Reducing URI expression renders LR cells proliferative, thereby accumulating c-MYC–dependent replicative stress and hence making them radiosensitive. In line with these findings, complete URI deletion causes LR cell death and disruption of intestinal architecture, leading to GIS. Therefore, URI-positive (URI^{high}) slow-cycling cells within the crypts constitute the facultative stem cell pool capable of repopulating the organ after ionizing radiation.

CONCLUSION: URI labels LR cells, which are essential for intestinal regeneration after high-dose irradiation. Reducing URI levels before ionizing radiation increases β–catenin–c-MYC–dependent proliferation and replicative stress-induced DNA damage, thereby rendering LR cells radiosensitive. On the basis of this work, selective c-MYC inhibition could be used as a countermeasure for humans at risk of developing radiation-induced GIS. ■

The list of author affiliations is available in the full article online.
*These authors contributed equally to this work.
†Corresponding author. Email: ndjouder@cnio.es
Cite this article as A. Chaves-Pérez *et al.*, *Science* **364**, eaaq1165 (2019). DOI: 10.1126/science.aaq1165

RESEARCH ARTICLE

TISSUE REGENERATION

URI is required to maintain intestinal architecture during ionizing radiation

Almudena Chaves-Pérez[1]*, Mahmut Yilmaz[1]†, Cristian Perna[2]†, Sergio de la Rosa[1]*, Nabil Djouder[1]*‡

Ionizing radiation (IR) can cause gastrointestinal syndrome (GIS), a lethal disorder, by means of unknown mechanisms. We show that high-dose irradiation increases unconventional prefoldin RPB5 interactor (URI) levels in mouse intestinal crypt, but organ regeneration correlates with URI reductions. URI overexpression in intestine protects mice from radiation-induced GIS, whereas halving URI expression sensitizes mice to IR. URI specifically inhibits β-catenin in stem cell–like label-retaining (LR) cells, which are essential for organ regeneration after IR. URI reduction activates β-catenin–induced c-MYC expression, causing proliferation of and DNA damage to LR cells, rendering them radiosensitive. Therefore, URI labels LR cells which promote tissue regeneration in response to high-dose irradiation, and c-MYC inhibitors could be countermeasures for humans at risk of developing GIS.

Gastrointestinal syndrome (GIS) is a lethal intestinal disorder that occurs after exposure to high-dose irradiation [>10 gray (Gy)] after uncontrolled release of radioactive materials or intensive radiotherapy for cancer treatment (*1*). Between 7 and 10 days after high-dose irradiation, intestinal mucosa is disrupted, leading to watery diarrhea, dehydration and electrolyte loss, gastrointestinal bleeding, and intestinal perforation. The breakdown of the epithelial barrier favors the translocation of bacteria into the bloodstream, leading to multisystem organ failure (*1*, *2*).

Under homeostatic conditions, rapid turnover of the intestinal epithelium is driven by leucine-rich repeat–containing G protein–coupled receptor 5–positive ($Lgr5^{+}$ or $Lgr5^{high}$) intestinal stem cells (ISCs) located at the base of the crypts (*3*). As $Lgr5^{high}$ ISCs divide, they migrate upward and undergo 4 to 5 replications, becoming $Lgr5^{low}$ progenitors or transit-amplifying (TA) cells committed to differentiation. Differentiated TA cells generate the villi, which are composed of intestinal epithelial cells (IECs), namely goblet cells, enteroendocrine cells, and nutrient-absorbing enterocytes (*4*). IECs continuously move upward to villus tips, where they undergo apoptosis within 5 to 7 days of formation (*4*). At the +4 position between bases of the crypts and TA cells, quiescent or low-proliferating "label-retaining" (LR) cells provide a reserve pool of stem cells if ISCs are depleted (*4*, *5*). LR cells are $Lgr5^{+}$ and have a secretory phenotype like Paneth cells, also located at the base of the crypts (*6*).

Gastrointestinal histopathological changes of chronic or high radiation doses include nuclear hyperchromasia and enlargement, mitotic arrest, death of rapidly proliferating crypt cells (ISCs and TA cells), epithelial surface area reductions, villous blunting, crypt hypoplasia, and fibrosis in submucosa, leading to ischemic lesions in the small bowel (*1*, *2*). In less susceptible patients, intestinal tissue has a great regenerative potential when exposed to acute irradiation. The intestinal regenerative response involves the activation of slow proliferative cells participating in the initial and rapid formation of regenerative areas (RAs). Within several days, the intestine is completely restored. Why some patients are more susceptible than others remains an unsolved question, and thus, quantitative biomarkers are needed to predict GIS susceptibility and assess degrees of intestinal injury.

Highly proliferative $Lgr5^{high}$ ISCs are radiosensitive (*7*–*9*). However, several reports indicate that $Lgr5^{+}$ cells are able to repopulate the crypt compartment after intense irradiation (*10*–*14*), possibly by means of activation and proliferation of the LR cells, suggesting that LR cells are crucial for regeneration of the injured tissue. Additionally, after intestinal injury, LR cells give rise to the main IECs, suggesting that LR quiescent cells constitute a clonogenic reservoir of stem cells that proliferate after tissue injury (*6*). Further elucidation of the contributions of crypt cells and the mechanisms leading to intestinal regeneration after injury is required.

The DNA damage checkpoint protein p53 modulates signaling pathways involved in ionizing radiation (IR) responses in mammalian cells (*8*, *15*). p53-deficient mice, which exhibit diminished crypt cell apoptosis, are still susceptible to IR injury, indicating that p53-induced apoptosis is not sufficient to cause GIS (*16*). Recent findings suggest that AIM2 (absent in melanoma 2) senses radiation-induced DNA damage in the nucleus, thereby inducing caspase-1–activating inflammasome formation, leading to pyroptosis and maturation of proinflammatory cytokine interleukin-1β (*17*). Clearly, mechanisms underlying GIS still remain poorly understood. There is thus a need to identify the genes required to maintain intestinal tissue architecture during IR and determine their function.

Abl affects URI levels in intestinal crypts

Previous studies suggest that unconventional prefoldin RPB5 interactor (URI) (*18*) controls and protects genome integrity in response to environmental insults (*19*, *20*). To elucidate the role of URI in GIS, we constructed a chamber with lead plates to irradiate the abdominal cavities of mice, mimicking radiotherapy procedures (fig. S1, A to D, and materials and methods). Experiments with the device indicated that mice survived abdominal irradiation (AbI) at doses that induce death and bone marrow failure (hematopoietic syndrome) when administered as whole-body irradiation (WBI) (fig. S1, E and F).

Ketamine- and xylazine-anesthesized C57BL/6 mice placed in this device (fig. S2A) were exposed to 2- to 6-Gy AbI doses and sacrificed 24 to 182 hours later (fig. S2B), and URI levels were examined by immunofluorescence (IF), quantitative real-time polymerase chain reaction (qRT-PCR), and Western blot (WB) analyses. Low doses (2 to 6 Gy) did not affect URI expression in intestinal crypts (fig. S2, C to M). However, intense AbI (8 to 14 Gy), dose-dependently increased URI levels, mainly in upper crypts, 24 to 48 hours postirradiation (figs. S2, H and I, and S3, A to J), correlating with increases in DNA damage response markers (fig. S3, B, G, I, and J). We detected a drop in URI expression in RAs from C57BL/6 mice, 72 to 96 hours after intense AbI (8 to 14 Gy) (figs. S2, L and M, and S3, K to N). However, when intestine was fully regenerated 182 hours postirradiation, URI levels tended to normalize to homeostasis levels (fig. S3, A to G). These data demonstrate that URI levels fluctuate time- and dose-dependently in intestinal crypts and suggest a correlation between decreased URI expression, highly proliferative cells, and the formation of RAs after intense IR.

URI overexpression protects against GIS

Hypothesizing that early increases in URI levels may protect the intestine from high irradiation, we generated a knock-in (KI) mouse [designated $hURI^{(+/KI)Int}$], expressing Flag-tagged human URI (hURI) via a tetracycline-dependent transactivator controlled by the villin promoter (fig. S4A). After 4 weeks on doxycycline treatment, $hURI^{(+/KI)Int}$ mice expressed hURI in the intestine from a single allele, at a level about six times greater than that of endogenous mouse URI (mURI). Notably, $hURI^{(+/+)Int}$ littermates lacked hURI expression (fig. S4, B to E).

[1]Cancer Cell Biology Programme, Growth Factors, Nutrients and Cancer Group, Centro Nacional Investigaciones Oncológicas, CNIO, Madrid 28029, Spain. [2]Department of Pathology, Hospital Universitario Ramón y Cajal, IRYCIS, Madrid 28034, Spain.
*Present address: Molecular Oncology Programme, Growth Factors, Nutrients and Cancer Group, Centro Nacional de Investigaciones Oncologicas, CNIO, Madrid 28029, Spain. †These authors contributed equally to this work.
‡Corresponding author. Email: ndjouder@cnio.es

hURI$^{(+/+)Int}$ and hURI$^{(+/KI)Int}$ mice had similar survival rates, normal body weights, and similar intestine lengths (fig. S4, F to H). However, longer villi were detected as hURI$^{(+/KI)Int}$ mice aged (fig. S4, I and J). Notably, hURI$^{(+/KI)Int}$ mice exhibited unchanged proliferative capacity, but increased differentiation, as they aged and when compared with URI$^{(+/+)Int}$ mice (fig. S4, K to Q).

To evaluate the responses of hURI$^{(+/KI)Int}$ mice to AbI, we determined the minimum AbI dose causing 70% lethality within 10 days (LD70/10), recapitulating GIS. About 70% of 22-Gy–abdominally irradiated C57BL/6 mice died within 10 days (fig. S5, A and B). hURI$^{(+/KI)Int}$ mice survived 22-Gy AbI for more than 25 days, whereas 70% of their control littermates died within 10 days (Fig. 1A). Moreover, losses of hURI$^{(+/KI)Int}$ mouse body weight and intestinal length were smaller, and, unlike hURI$^{(+/+)Int}$ mice, hURI$^{(+/KI)Int}$ mice showed no signs of diarrhea 10 days postirradiation (fig. S6, A to C). Bromodeoxyuridine-positive (BrdU^{+}) surviving crypts were increased in hURI$^{(+/KI)Int}$ mice 96 hours post-AbI (fig. S6D). Additionally, 22-Gy–abdominally irradiated hURI$^{(+/KI)Int}$ mice had normal intestinal architecture with better regenerative capacity and increased differentiation than irradiated hURI$^{(+/+)Int}$ mice (Fig. 1B and fig. S6, E to I). Thus, hURI overexpression protects intestines from lethal IR doses. However, increasing radiation doses to 26 Gy caused similar body weight loss, intestinal length reduction, diarrhea, and death in hURI$^{(+/+)Int}$ and hURI$^{(+/KI)Int}$ mice (Fig. 1, A and B, and fig. S6, A to C).

URI loss causes intestinal failure

Next, we crossed URI conditional knockout (URI lox) and Villin-creERT2 mice to explore the consequences of knocking out URI expression in intestinal epithelium (fig. S7, A to C). Activation of creERT2 recombinase under control of the *Villin* promoter was induced by dietary provision of

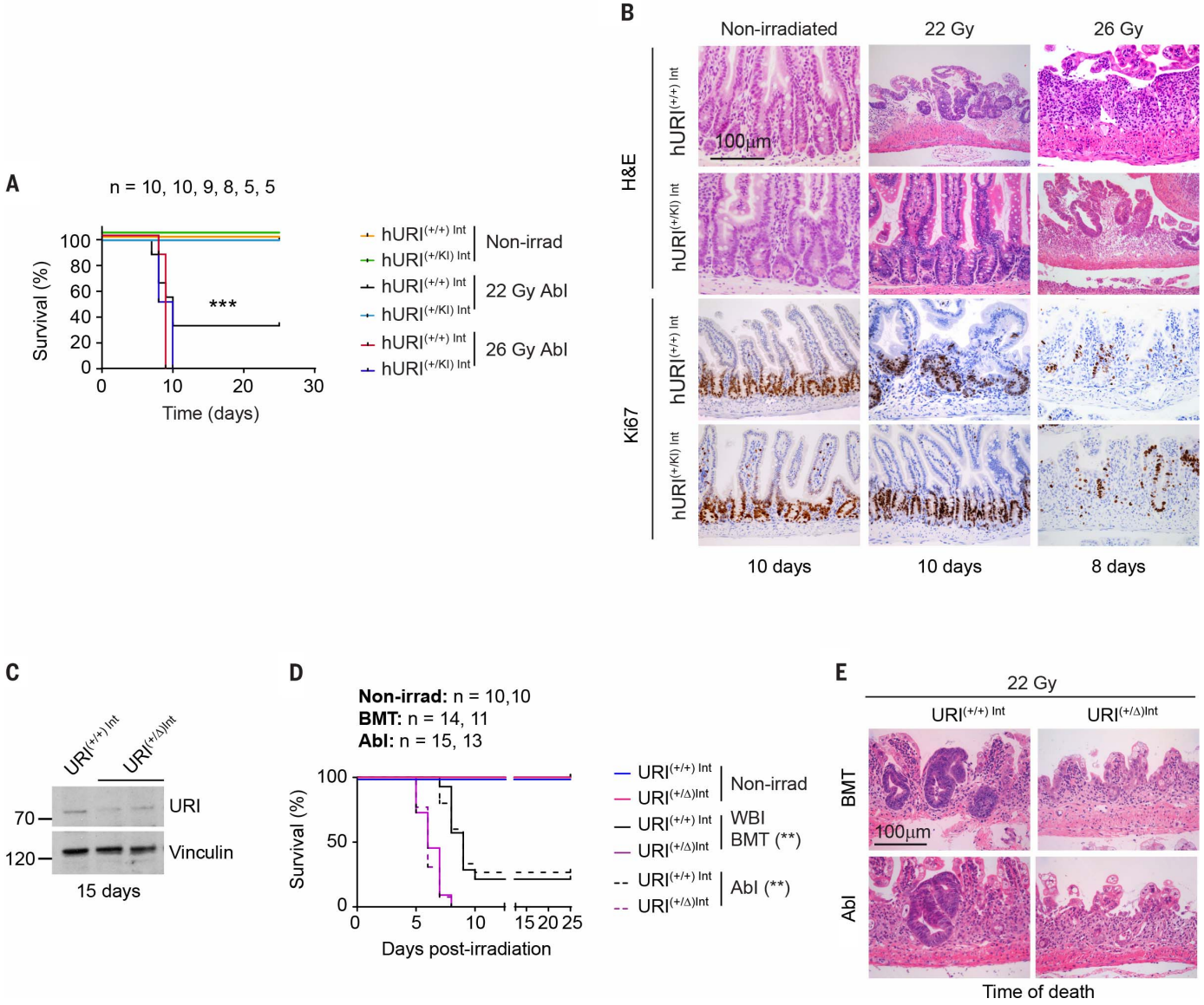

Fig. 1. URI safeguards intestine after high-dose irradiation. (**A**) Kaplan-Meier curve of nonirradiated hURI$^{(+/+)Int}$ and hURI$^{(+/KI)Int}$ mice, and 22- and 26-Gy–abdominally irradiated hURI$^{(+/+)Int}$ and hURI$^{(+/KI)Int}$ mice. (**B**) Hematoxylin and eosin (H&E) staining and immunohistochemistry analysis in nonirradiated hURI^{Int} and 22- and 26-Gy–abdominally irradiated hURI^{Int} intestinal sections at time of death (8 to 10 days). (**C**) WB of intestines from URI^{Int} mice after 15 days of tamoxifen treatment. Numbers to the left of the blot are in kDa. (**D**) Kaplan-Meier curve of URI$^{(+/+)Int}$ and URI$^{(+/Δ)Int}$ mice after 15 days of tamoxifen treatment, bone marrow–transplanted (BMT) URI$^{(+/+)Int}$ mice, URI$^{(+/Δ)Int)}$ mice, and 22-Gy–abdominally irradiated URI$^{(+/+)Int}$ and URI$^{(+/Δ)Int}$ mice. (**E**) H&E staining in intestinal sections from bone marrow–transplanted and 22-Gy–abdominally irradiated URI^{Int} mice. Data represent mean ± SEM. In (A) and (D), $^{**}P < 0.01$ and $^{***}P < 0.001$ by Mantel-Cox test analysis.

tamoxifen to 8-week-old mice, yielding URI$^{(+/+)Int}$, URI$^{(+/\Delta)Int}$, and URI$^{(\Delta/\Delta)Int}$ mice (where Δ indicates deletion). URI was specifically ablated in intestinal epithelium after 2 and 6 days in URI$^{(\Delta/\Delta)Int}$ mice and, after 15 days in URI$^{(+/\Delta)Int}$ mice (fig. S7, D to F). URI$^{(\Delta/\Delta)Int}$ mice died within 7 to 9 days of tamoxifen treatment, like 22-Gy–abdominally irradiated C57BL/6 mice, mimicking GIS, but unlike their URI$^{(+/+)Int}$ or heterozygous URI$^{(+/\Delta)Int}$ littermates (fig. S7, G to H). URI$^{(\Delta/\Delta)Int}$ mice also had reduced body weight, intestinal length, and blood glucose levels (similar to 22-Gy–abdominally irradiated C57BL/6 mice), whereas no clear phenotypic changes were observed in URI$^{(+/+)Int}$ and URI$^{(+/\Delta)Int}$ mice at this stage (fig. S7, I to K). Both URI$^{(\Delta/\Delta)Int}$ and 22-Gy–abdominally irradiated C57BL/6 mice had dilated stomachs with accumulated food and grossly swollen small intestines with no luminal content at death (fig. S7L), suggesting normal food access but possible gastric outlet obstruction.

After 6 days of tamoxifen treatment, URI$^{(\Delta/\Delta)Int}$ mice had normal intestinal tissue architecture, but their crypts showed nuclear hyperchromasia, cell flattening, and signs of cell death (fig. S7, M and N). After 7 to 9 days, they showed drastic reductions in villus length, crypt hypoplasia, destruction of intestinal architecture, and loss of epithelial surface, as also seen in 22-Gy–abdominally irradiated C57BL/6 mice (fig. S7, M to O). Increased sirius red, Masson trichrome, and reticulin staining in both models revealed fibrotic intestines (fig. S8, A and B).

Moreover, compared with control littermates, URI$^{(\Delta/\Delta)Int}$ mice exhibited defects in terminally differentiated enterocytes, goblet cells, and enteroendocrine cells after 6 days of tamoxifen treatment (fig. S9, A to H). Lysozyme staining revealed no differences in Paneth cell number between URI$^{(+/+)\ Int}$ and URI$^{(\Delta/\Delta)Int}$ mice (fig. S9, I to K). Furthermore, local and systemic inflammation (fig. S10, A and B) and signs of bacteremia (fig. S10, C to F) were detected in URI$^{(\Delta/\Delta)Int}$ mice at death (but not at 2 days after tamoxifen treatment) and 22-Gy–abdominally irradiated C57BL/6 mice at 72 hours postirradiation. Finally, fluorescein isothiocyanate–dextran (FITC-dextran) assays and IF analysis of β-actin and zonula occludens (ZO-1) in URI$^{(\Delta/\Delta)Int}$ intestines (fig. S10, G and H) indicated loss of epithelial integrity in both models. These findings suggest that URI loss disrupts murine intestinal architecture, possibly leading to septic shock and death of mice. Thus, URI$^{(\Delta/\Delta)Int}$ mice seem to recapitulate GIS.

Halving URI sensitizes to GIS

Additional markers of stress were detected in intestinal epithelium of URI$^{(\Delta/\Delta)Int}$ and 22-Gy–abdominally irradiated C57BL/6 mice (fig. S11, A to J). URI$^{(+/\Delta)Int}$ mice exhibited increased DNA damage response markers in the intestine after 15 days of tamoxifen treatment (fig. S12, A to E). Furthermore, proliferation markers were increased in URI$^{(+/\Delta)Int}$ crypts (fig. S12, F to I).

To check whether URI$^{(+/\Delta)Int}$ mice were sensitized to IR, we abdominally irradiated URI$^{(+/+)Int}$ and URI$^{(+/\Delta)Int}$ mice with 6, 10, and 14 Gy (fig. S13A). At these doses, mouse survival was not affected after AbI (fig. S13B). However, high AbI doses (14 Gy) significantly reduced URI$^{(+/\Delta)Int}$ mouse body weight, intestinal length, and villi length and affected intestinal architecture when compared with nonirradiated URI$^{(+/\Delta)Int}$ mice and abdominally irradiated URI$^{(+/+)Int}$ littermate controls (fig. S13, C to G). Additionally, increased intestinal permeability was detected in URI$^{(+/\Delta)Int}$ mice when compared with their littermate controls, but these effects were further amplified in abdominally irradiated URI$^{(+/\Delta)Int}$ mice (fig. S13 H).

Irradiation with 6 and 10 Gy significantly increased DNA damage and proliferation in abdominally irradiated URI$^{(+/\Delta)Int}$ mice when compared with nonirradiated URI$^{(+/\Delta)Int}$ mice and irradiated URI$^{(+/+)Int}$ littermate controls, 96 hours postirradiation (fig. S14, A to D). Notably, 14-Gy AbI doses in URI$^{(+/\Delta)Int}$ mice further amplified DNA damage increases when compared with 6- and 10-Gy doses (fig. S14, A and B). Consequently, intestinal regenerative capacity was impaired in 14-Gy–abdominally irradiated URI$^{(+/\Delta)Int}$ mice (fig. S14, D and E), which also had lower differentiation capacity when compared with nonirradiated URI$^{(+/\Delta)Int}$ mice (fig. S14, F to I). Thus, effects seen in URI$^{(+/\Delta)Int}$ mice are further strengthened after AbI (fig. S14J), indicating that URI$^{(+/\Delta)Int}$ mice are sensitized to IR.

Therefore, we checked effects of the LD70/10 dose in URI$^{(+/\Delta)Int}$ mice. When exposed to 22-Gy AbI, these mice presented signs of severe diarrhea and lower survival rates, body weight, and intestinal RAs than URI$^{(+/+)Int}$ littermate controls (Fig. 1, C to E, and fig. S15, A and C). To check that 22-Gy–abdominally irradiated mice died from GIS rather than hematopoietic syndrome, bone marrow from Tg.CAG–EGFP (Tg., transgenic; CAG, CMV enhancer, chicken β-actin promoter and rabbit β-globin splice acceptor site; EGFP, enhanced green fluorescent protein) mice was transplanted into 22-Gy WBI URI$^{(+/+)Int}$ and URI$^{(+/\Delta)Int}$ mice (fig. S15, D and E). Transplanted mice had similar phenotypes to 22-Gy–abdominally irradiated mice (Fig. 1, D and E, and fig. S15, B and C). Thus, URI$^{(+/\Delta)Int}$ mice are sensitized to GIS and have a reduced life span.

URI is expressed in Lgr5^{low} cells

The above findings suggest that URI loss may specifically affect intestinal cells required for tissue regeneration after injury. IF analysis of intestines of Lgr5-EGFP-IRES-creERT2 (IRES, internal ribosome entry site; creERT2, Cre recombinase estrogen receptor type 2) and C57BL/6 mice showed that URI was predominantly expressed in the upper part of the crypts, colocalizing with its binding partner heat shock protein 90 (HSP90) (*18*), and not in Sox9^{+} cells, Paneth cells, or villi (fig. S16, A to G, and movie S1). Separation of Lgr5^{low} (TA) cells and Lgr5^{high} ISCs from Lgr5-EGFP-IRES-creERT2 mice by fluorescence-activated cell sorting confirmed enrichment of URI in Lgr5^{low} cells (fig. S16, H to J).

To further check URI localization, we generated a URI-creERT2-IRES-EGFP knock-in mouse model carrying a creERT2-IRES-EGFP cassette under control of the *Uri* promoter (fig. S17, A to E). Heterozygous mice harbor a URI-creERT2-IRES-EGFP knock-in allele that abolishes *Uri* gene function and expresses creERT2 and EGFP proteins. We detected no EGFP signal in URI-creERT2-IRES-EGFP mice by standard IF (fig. S17F), possibly because the IRES element may affect EGFP expression. However, staining for cre recombinase confirmed that URI was mainly localized in the upper part of the crypts and not in Paneth cells (fig. S17G).

Slow-cycling cells are URI^{+}

To check the role of URI^{+} cells during homeostasis, we crossed URI-creERT2-IRES-EGFP and reporter R26-stop–EYFP (enhanced yellow fluorescent protein) mice to generate URI-creERT2;R26-stop-EYFP mice (Fig. 2A). URI^{+} cells expressed an inducible cre recombinase that specifically deleted the *loxP*-flanked stop cassette in the Rosa26R reporter locus in the URI-expressing cells of the offspring. All descendants of the labeled cells thus inherited EYFP. IF analysis from mice injected with 4-hydroxytamoxifen (4-OHT) for five consecutive days showed that EYFP cells were present in the upper part of the crypts (Fig. 2, B and C). Moreover, villi originating from EYFP^{+} TA cells were also EYFP^{+} (Fig. 2, B and C), suggesting full recombination.

Next, we labeled URI^{+} cells in URI-creERT2;R26-stop-EYFP mice that were injected with 4-OHT for five consecutive days, and then tamoxifen treatment was stopped for 1 week to enable complete organ regeneration (Fig. 2, A and B). IF showed that 95% of EYFP^{+} cells in the crypt were slow-cycling cells (Fig. 2, C to F), most likely corresponding to LR cells. Notably, because Lgr5^{high} ISCs were EYFP^{-} before tracing (Fig. 2C), all descendant cells from Lgr5^{high} ISCs were also EYFP^{-} (Fig. 2C), suggesting that highly proliferative Lgr5^{high} ISCs are the cells at the origin of organ regeneration, excluding the role of slow-cycling URI^{+} cells under homeostatic conditions.

We also crossed the URI-creERT2-IRES-EGFP mouse with the transgenic reporter CAG-Katushka mouse, which expresses the far-red fluorescent protein Katushka, driven by the hybrid CAG promoter upon cre-mediated recombination. To label URI^{+} cells, URI-creERT2;CAG-Katushka mice were injected with 4-OHT for five consecutive days (Fig. 2, G and H). Katushka^{+} cells were detected in the upper part of the crypts (Fig. 2I), and endogenous EGFP was detected after signal amplification colocalized with Katushka^{+} cells (fig. S17H). Moreover, slow-cycling cells were Katushka^{+} (Fig. 2J). Stopping tamoxifen treatment for 1 week to allow organ regeneration and qRT-PCR analysis of sorted Katushka^{+} cells indicated that these cells were URI^{+}Lgr5^{medium} and were slow-cycling cells, most likely corresponding to LR cells (Fig. 2, K to M, and fig. S17I).

URI labels intestinal LR cells

To test whether LR cells express URI, we performed pulse-chase labeling with a tetracycline operator (TetO)–regulated H2B–GFP (histone 2B–green fluorescent protein) fusion protein. TetO-H2B-GFP (H2B-GFP) mice were crossed

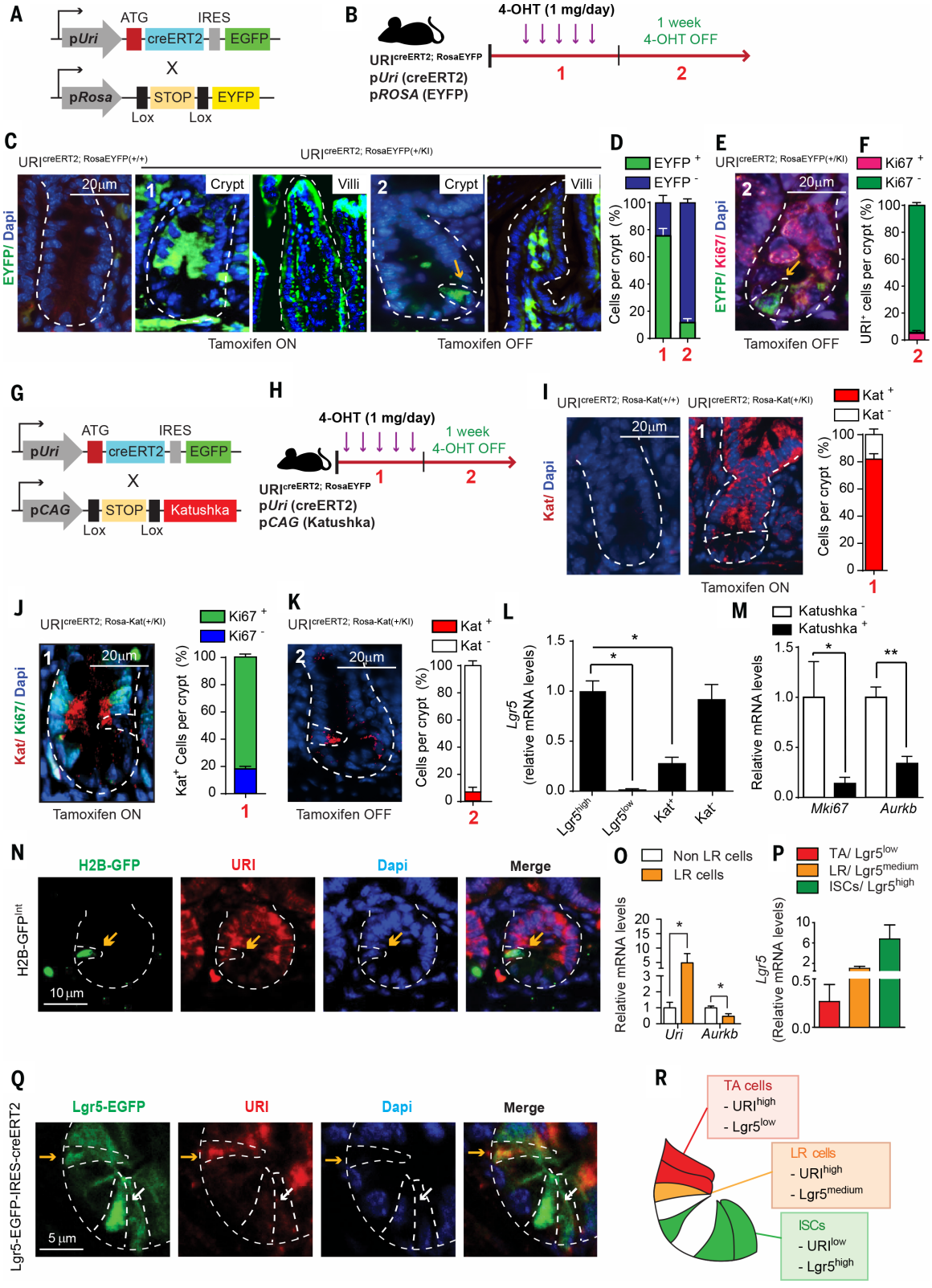

Fig. 2. URI labels intestinal LR cells. (**A**) Schematic showing the cross between URI-creERT2-IRES-EGFP and R26-stop-EYFP mice. (**B**) Experimental design to express EYFP in URI$^+$ cells. (**C** and **D**) IF (C) and quantification (D) of EYFP in intestinal sections from experiments described in (B). In (C), the orange arrow indicates URI-positive slow-cycling cells. Dapi, 4′,6-diamidino-2-phenylindole. (**E** and **F**) Co-IF (E) and quantification (F) of EYFP and Ki67 in intestinal sections from the labeling experiment in URI-creERT2;R26-stop-EYFP mice. (**G**) Schematic showing the cross between URI-creERT2-IRES-EGFP and CAG-stop-Katushka mice. (**H**) Experimental design to express Katushka in URI$^+$ cells. (**I**) IF and quantification of Katushka (Kat) in intestinal sections from the labeling experiment in URI-creERT2;CAG-Katushka mice. (**J**) Co-IF and quantification of Katushka and Ki67 in intestinal sections from the labeling experiment in URI-creERT2;CAG-Katushka mice. (**K**) IF and quantification of Katushka in intestinal sections from the tracing experiment in URI-creERT2;CAG-Katushka mice. (**L** and **M**) qRT-PCR of *Lgr5* (L) and proliferation markers (*Mki67* and *Aurkb*) (M) in sorted Katushka$^+$ and Katushka$^-$ cells. Sorted Lgr5^{high} and Lgr5^{low} cells from Lgr5-GFP-IRES-creERT2 mice were used as controls (n = 3 per group). (**N**) Co-IF of H2B-GFP and URI in intestinal sections from H2B-GFP^{Int} mice. The orange arrows indicate LR cells. (**O**) qRT-PCR of intestinal GFP$^+$ and GFP$^-$ cells sorted from H2B-GFP^{Int} mice (n = 3 per group). (**P**) qRT-PCR of Lgr5^{high} and Lgr5^{low} cells and LR cells sorted from Lgr5-GFP-IRES-CreERT2 and H2B-GFP^{Int} mice, respectively (n = 3 per group). (**Q**) Co-IF of Lgr5-GFP and URI in intestinal sections from Lgr5-GFP-IRES-CreERT2 mice. White and orange arrows show Lgr5$^+$URI$^-$ cells and Lgr5$^+$URI$^+$ cells, respectively. (**R**) Crypt schematic depicting URI location. Data represent mean ± SEM. In (L), (M), (O), and (P), $^*P < 0.05$ and $^{**}P < 0.01$ by Student's t test analysis. Quantification was performed for more than 50 crypts per mouse in three independent mice. Dashed white lines represent crypts.

with Villin-rtTA2-M2 transgenic mice, generating H2B-GFP^{Int} mice, in which H2B-GFP can be pulse-chased during aging (fig. S18, A and B). H2B-GFP protein expression was monitored after 2 weeks of doxycycline (Doxy ON) pulsing (fig. S18C) and a subsequent 3-week (Doxy OFF) chase in H2B-GFP^{Int} mice aged 8 to 10 weeks, revealing that 74.67 ± 0.56% of H2B-GFP$^+$ cells were URI-positive (URI$^+$) (Fig. 2N and fig. S18D). Notably, some H2B-GFP$^+$ cells were also URI$^-$, possibly Paneth cells, which are replaced every 20 to 23 days (fig. S18, D and E). Sorting of LR and non-LR cells confirmed that LR cells were URI$^+$ (Fig. 2O and fig. S18F). Furthermore, Lgr5 expression was evaluated by qRT-PCR in sorted LR cells from H2B-GFP mice and compared with sorted Lgr5^{low} (TA) cells and Lgr5^{high} ISCs from Lgr5-EGFP-IRES-creERT2 mice, demonstrating that LR cells express a medium level of Lgr5 (Lgr5^{medium} cells). So, URI$^+$ LR cells might be considered as Lgr5$^+$ or Lgr5^{medium} cells (Fig. 2P). Additional studies on Lgr5-EGFP-IRES-creERT2 mice revealed a discrete URI-expressing subpopulation in Lgr5$^+$ cells (Fig. 2, Q and R). Thus, URI marks LR cells under homeostatic conditions.

URI$^+$ LR cells are radioresistant

To analyze the behavior of URI$^+$Lgr5$^+$ cells after IR, Lgr5-EGFP-IRES-creERT2 mice were exposed to 14- and 22-Gy irradiation and sacrificed 24 hours later (Fig. 3A). The GFP signal was significantly reduced in most intestinal cells, but co-IF analysis revealed some surviving GFP$^+$ cells expressing URI after 14-Gy irradiation (Fig. 3B and fig. S19A), suggesting that 14-Gy-IR–resistant Lgr5$^+$ cells are URI$^+$. A lethal dose of 22-Gy AbI in Lgr5-EGFP-IRES-creERT2 mice blunted GFP$^+$ signals (Fig. 3B and fig. S19A).

We next checked the effects of IR on LR cells in H2B-GFP^{Int} mice (Fig. 3C). Numbers of H2B-GFP$^+$ cells were unchanged in 14-Gy irradiated H2B-GFP^{Int} mice 24 hours postirradiation, and surviving LR cells expressed URI (Fig. 3D and fig. S19B), suggesting that URI$^+$ LR cells are radioresistant. However, 22-Gy irradiation killed all GFP signals (Fig. 3, C and D, and fig. S19B). Notably, at 48 to 72 hours after 14-Gy irradiation, reduced URI levels were detected specifically in highly proliferative LR cells on the basis of co-IF analysis (Fig. 3, C and D, and fig. S19C), suggesting that reduced URI expression in quiescent LR cells may render these cells highly proliferative.

URI$^+$ cells repopulate the intestine after IR

To check whether URI$^+$ cells (TA and slow-cycling URI$^+$ cells) regenerated the intestinal epithelium after AbI, URI-creERT2;R26-stop-EYFP mice were injected with 4-OHT for five consecutive days before 14-Gy IR (fig. S19D). IF analysis indicated that 97.27 ± 1.42% of cells in RAs were EYFP$^+$ 96 hours postirradiation (fig. S19D). Thus, URI$^+$ cells (TA and/or slow-cycling URI$^+$ cells) regenerate the intestine after 14-Gy IR.

To determine the contribution of slow-cycling URI$^+$ cells in intestinal regeneration, URI-creERT2;R26-stop-EYFP mice were injected with 4-OHT for five consecutive days, tamoxifen treatment was stopped for 1 week, and then the mice were finally subjected to 14-Gy AbI (Fig. 3E). EYFP$^+$ cells (93.7%) were detected in RAs and in incipient villi 96 hours postirradiation (Fig. 3, F and G). Further IF analysis in RAs indicated that URI$^+$ (EYFP$^+$) cells gave raise to different cell populations, representing cell lineages present in the crypts during homeostasis (Fig. 3H). Lgr5^{high} ISCs may then emanate from the slow-cycling URI$^+$ cells after IR. Additionally, EYFP$^+$ cells stained for differentiation markers in the newly formed villi (Fig. 3, I and J). Similar results were observed with 14-Gy–abdominally irradiated URI-creERT2;CAG-Katushka mice (fig. S19, E to I). Thus, slow-cycling URI$^+$ cells, most likely LR cells, constitute a predominant facultative stem cell pool capable of repopulating the organ after injury and when Lgr5^{high} ISCs are damaged (Fig. 3K).

URI protects LR cells from IR

Next, to check whether reduced URI levels sensitized LR cells to IR, we crossed URI$^{(+/\Delta)Int}$ and URI$^{(\Delta/\Delta)Int}$ mice with H2B-GFP^{Int} mice, generating URI$^{(+/\Delta)Int\text{-}H2B\text{-}GFP}$ and URI$^{(\Delta/\Delta)Int\text{-}H2B\text{-}GFP}$ mice, respectively. IF analysis of crypts and qRT-PCR of sorted LR cells from URI$^{(+/\Delta)Int\text{-}H2B\text{-}GFP}$ mice after 15 days of tamoxifen treatment confirmed that halving URI levels rendered LR cells more proliferative, accumulating replicative stress and DNA damage in the absence of IR (Fig. 4, A to C, and fig. S20, A to C). When we administered 14-Gy AbI doses in URI$^{(+/\Delta)Int\text{-}H2B\text{-}GFP}$ mice, we detected apoptotic LR cells within 24 hours, significantly reducing LR cell counts (Fig. 4, D to F), although this dose did not kill LR cells in URI$^{(+/+)Int\text{-}H2B\text{-}GFP}$ mice. Thus, reduced URI expression in LR cells increases proliferation and DNA damage, rendering these cells radiosensitive. IF analysis indicated that LR cells from URI$^{(\Delta/\Delta)Int\text{-}H2B\text{-}GFP}$ mice were apoptotic after 4 days of tamoxifen treatment (Fig. 4, G to I).

We therefore determined whether URI overexpression protects LR cells against IR by crossing hURI$^{(+/KI)Int}$ and H2B-GFP mice to obtain hURI$^{(+/KI)Int\text{-}H2B\text{-}GFP}$ mice. To this end, we delivered 22-Gy AbI doses because, at this dose, LR cells died (Fig. 3, C and D). LR cells survived 22-Gy AbI in hURI$^{(+/KI)Int\text{-}H2B\text{-}GFP}$ mice, but not in hURI$^{(+/+)Int\text{-}H2B\text{-}GFP}$ mice (Fig. 4, J to M), demonstrating that the increased regenerative capacity of 22-Gy–abdominally irradiated hURI$^{(+/KI)Int}$ mice described in Fig. 1C is due to an increased number of surviving LR cells. We therefore checked whether URI might protect against IR by interfering with DNA repair machinery by means of either nonhomologous end joining (NHEJ) or homologous recombination (HR). To test this possibility, HCT-116 (human colon cancer) cells were stably transfected with fluorescent reporter constructs containing a *GFP* gene with recognition sites for a rare-cutting I-SceI endonuclease to induce double-strand breaks (*21*). Successful repair of the I-SceI–induced breaks by NHEJ or HR restores the functional *GFP* gene, and numbers of GFP-positive cells detected by flow cytometry provide quantitative measures of NHEJ or HR efficiency. Applying this method to HCT-116 cells in which URI was silenced or overexpressed revealed that URI is involved in double-strand break repair by NHEJ (fig. S21, A to F).

We also analyzed the behavior of Lgr5^{high} ISCs after IR in hURI$^{(+/KI)Int}$ mice. Hence, we crossed Lgr5-EGFP-IRES-creERT2 and hURI$^{(+/KI)Int}$ mice to generate hURI$^{(+/KI)Int\text{-}Lgr5\text{-}EGFP}$ mice. IF analysis indicated that Lgr5^{high} ISCs died in 22-Gy–abdominally irradiated hURI$^{(+/KI)Int\text{-}Lgr5\text{-}EGFP}$ mice (Fig. 4, N to P). Thus, URI overexpression specifically radio-protects LR cells, but not highly proliferative Lgr5^{high} ISCs.

To determine whether URI loss also affects the proliferation status of TA cells, we crossed URI$^{(+/+)Int}$ and URI$^{(\Delta/\Delta)Int}$ mice with Lgr5-EGFP-IRES-creERT2 mice, generating URI$^{(+/+)Int\text{-}Lgr5\text{-}EGFP}$ and URI$^{(\Delta/\Delta)Int\text{-}Lgr5\text{-}EGFP}$ offspring, respectively (fig. S22, A to C). Analysis of isolated Lgr5^{low} TA cells from URI$^{(\Delta/\Delta)\ Int\text{-}Lgr5\text{-}EGFP}$ mice demonstrated that URI reductions increased TA proliferation (fig. S22, D and E) and reduced levels of lineage-specific transcription factors in TA cells after 6 days of tamoxifen treatment (fig. S22F). Moreover, despite p53 stabilization, Lgr5^{low} TA cells from URI$^{(\Delta/\Delta)\ Int\text{-}Lgr5\text{-}EGFP}$ mice exhibited enhanced BrdU incorporation, cyclin D1 levels, and retinoblastoma protein phosphorylation after 6 days of tamoxifen treatment (fig. S22, G to I). Further IF analyses indicated that Lgr5^{low} TA cells from URI$^{(\Delta/\Delta)\ Int\text{-}Lgr5\text{-}EGFP}$ mice entered apoptosis, but not Lgr5^{high} ISCs (fig. S22, J to L). Thus, proliferative TA cells may accumulate DNA damage and die after URI loss. Notably, co-staining of p53 and Ki67 (a cell proliferation marker) in URI$^{(\Delta/\Delta)Int}$ mice indicated that some TA cells proliferate and may escape from p53-induced cell cycle arrest and cell death (fig. S22M). Consequently, Lgr5^{low} cell numbers did not change in URI$^{(\Delta/\Delta)Int\text{-}Lgr5\text{-}EGFP}$ mice (fig. S22N), possibly because of cell death and proliferation, both of which normalized cell number after 6 days of tamoxifen treatment.

URI loss activates the β-catenin–c-MYC axis in LR cells

Increased proliferation and decreased differentiation suggested that reducing URI activates WNT–β-catenin signaling in TA and LR cells. Accordingly, analysis of gene expression in LR cells sorted from URI$^{(+/+)Int\text{-}H2B\text{-}GFP}$ and URI$^{(+/\Delta)Int\text{-}H2B\text{-}GFP}$ mice revealed significant increases in ISC markers (*Olfm4* and *Lgr5*) and activation of WNT–β-catenin target genes (*c-Myc* and *Ascl2*) in URI$^{(+/\Delta)Int\text{-}H2B\text{-}GFP}$ mice after 15 days of tamoxifen treatment (Fig. 5, A and B). IF analysis confirmed expression of c-MYC and Axin 2 in URI$^{(+/\Delta)Int\text{-}H2B\text{-}GFP}$ LR cells (Fig. 5, C to F). Similar patterns were observed in Lgr5^{low} (TA) cells sorted from URI$^{(+/+)Int\text{-}Lgr5\text{-}EGFP}$ and URI$^{(\Delta/\Delta)Int\text{-}Lgr5\text{-}EGFP}$ mice (fig. S23, A and B). WNT–β-catenin activation was corroborated by WB and immunohistochemistry analyses from URI$^{(\Delta/\Delta)Int}$ crypts (fig. S23, C and D). Notably, *c-Myc* expression was increased in the early stages of URI deletion (2 days), but apoptosis was not detected, correlating with increased proliferation

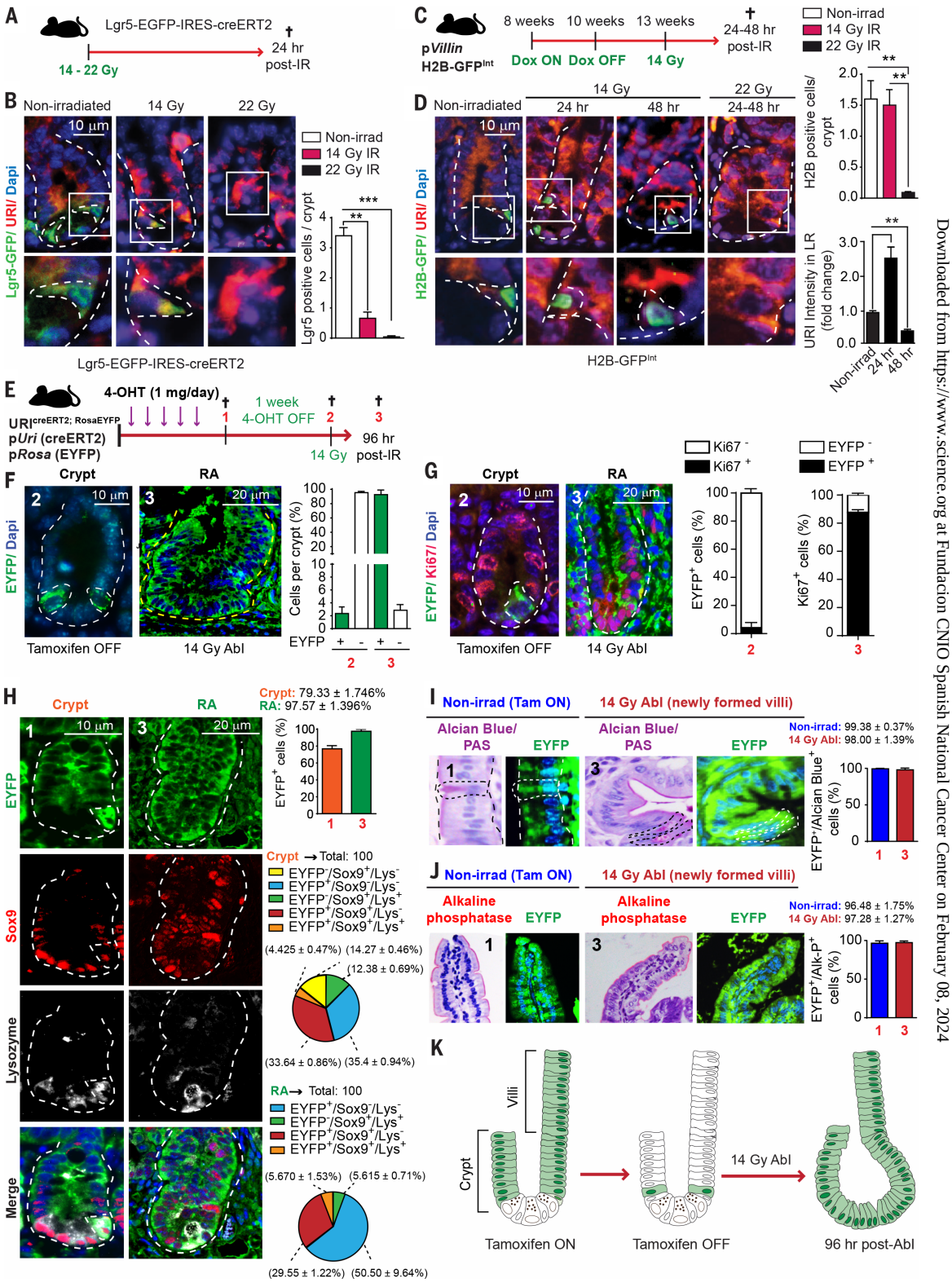

Fig. 3. URI$^+$ cells repopulate the intestine after IR. (**A**) Schematic showing the AbI procedure for Lgr5-GFP-IRES-CreERT2 mice. (**B**) Representative co-IF (left) for Lgr5-GFP and URI and quantifications (right) in intestinal sections from non-irradiated, 14- and 22-Gy–abdominally irradiated Lgr5-GFP-IRES-CreERT2 mice 24 hours postirradiation. (**C**) Schematic showing the experiment for pulse-chased and irradiated H2B-GFP^{Int} mice. (**D**) Representative co-IF (left) of H2B-GFP and URI and quantifications (right) in intestinal sections from nonirradiated, 14- and 22-Gy–abdominally irradiated H2B-GFP^{Int} mice at the indicated time points postirradiation. (**E**) Experimental design for tracing URI$^+$ cells after AbI. (**F**) Representative IF of EYFP and quantification of URI$^+$ cells in intestinal sections from labeled or 14-Gy–abdominally irradiated URI-creERT2;R26-stop-EYFP mice. (**G**) Representative IF of EYFP and Ki67 and quantification of URI$^+$KI67$^+$ cells. (**H**) Representative co-IF and quantification of EYFP, Sox9, and lysozyme in intestinal sections from nonirradiated and 14-Gy–abdominally irradiated URI-creERT2;R26-stop-EYFP mice 96 hours postirradiation. (**I** and **J**) Representative Alcian blue–periodic acid Schiff (PAS) (I) and alkaline phosphatase (J) staining and EYFP IF, as well as quantification, in consecutive intestinal sections from nonirradiated and 14-Gy–abdominally irradiated URI-creERT2;R26-stop-EYFP mice 96 hours postirradiation. Tam, tamoxifen. (**K**) Schematic showing the contribution of URI$^+$ cells to intestinal regeneration after 14-Gy AbI. Data represent mean ± SEM. In (B) and (D), $^{**}P < 0.01$ and $^{***}P < 0.001$ by Student's *t* test analysis. Quantification was performed over 50 crypts or 100 villi per mouse in three independent mice. Dashed white lines represent RAs.

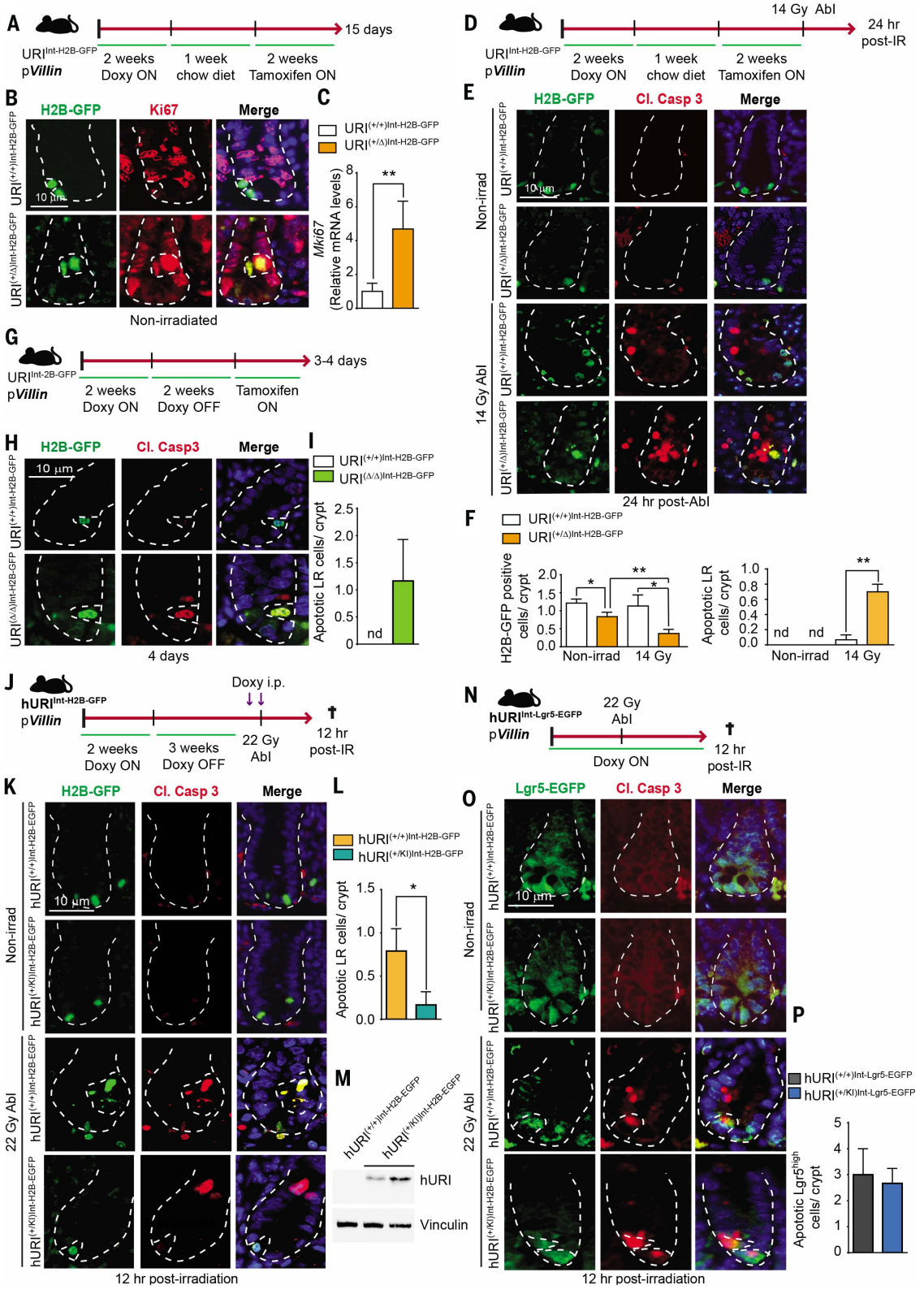

Fig. 4. URI protects LR cells from IR. (**A**) Schematic showing the experiment for pulse-chased URI$^{(+/\Delta)Int\text{-}H2B\text{-}GFP}$ mice. (**B** and **C**) Co-IF of H2B-GFP and Ki67 in intestinal sections (B) and qRT-PCR of *Mki67* of sorted LR cells (C) from pulse-chased URI$^{Int\text{-}H2B\text{-}GFP}$ mice after 15 days of tamoxifen treatment (n = 3 per group). (**D**) Schematic showing the experiment for pulse-chase labeling followed by 14-Gy AbI in hURI$^{H2B\text{-}GFP}$ mice. (**E** and **F**) Co-IF of H2B-GFP and cleaved caspase-3 (Cl. Casp 3) (E) and quantification of H2B-GFP^{+} cells per crypt and apoptotic LR cells per crypt (F) in intestinal sections from nonirradiated and 14-Gy–abdominally irradiated hURI$^{H2B\text{-}GFP}$ mice. (**G**) Schematic showing the experiment for pulse-chased URI$^{(\Delta/\Delta)Int\text{-}H2B\text{-}GFP}$ mice. (**H** and **I**) Co-IF of H2B-GFP and Cl. Casp3 (H) and quantification (I) in intestinal sections from pulse-chased URI$^{Int\text{-}H2B\text{-}GFP}$ mice. (**J**) Schematic showing pulse-chase labeling followed by 22-Gy AbI in hURI$^{Int\text{-}H2B\text{-}GFP}$ mice. i.p., intraperitoneal administration. (**K** and **L**) Co-IF of H2B-GFP and Cl. Casp3 (K) and quantification of apoptotic LR cells (L) in intestinal sections from nonirradiated and 22-Gy–abdominally irradiated hURI$^{Int\text{-}H2B\text{-}GFP}$ mice. (**M**) WB of hURI$^{Int\text{-}H2B\text{-}GFP}$ intestines after intraperitoneal injections of doxycycline. (**N**) Schematic showing the experiment for 22-Gy–abdominally irradiated hURI$^{Int\text{-}Lgr5\text{-}EGFP}$ mice sacrificed 12 hours post-irradiation. (**O** and **P**) Co-IF of H2B-GFP and Cl. Casp3 (O) and quantification of apoptotic Lgr5^{high} cells (P) in intestinal sections from 22-Gy–abdominally irradiated hURI$^{Int\text{-}Lgr5\text{-}EGFP}$ mice 12 hours postirradiation. Data represent mean ± SEM. In (C), (F), (I), (L), and (P), *P < 0.05 and **P < 0.01 by Student's t test analysis. Quantification was performed over 50 crypts per mouse in three independent mice. Dashed white lines represent RAs.

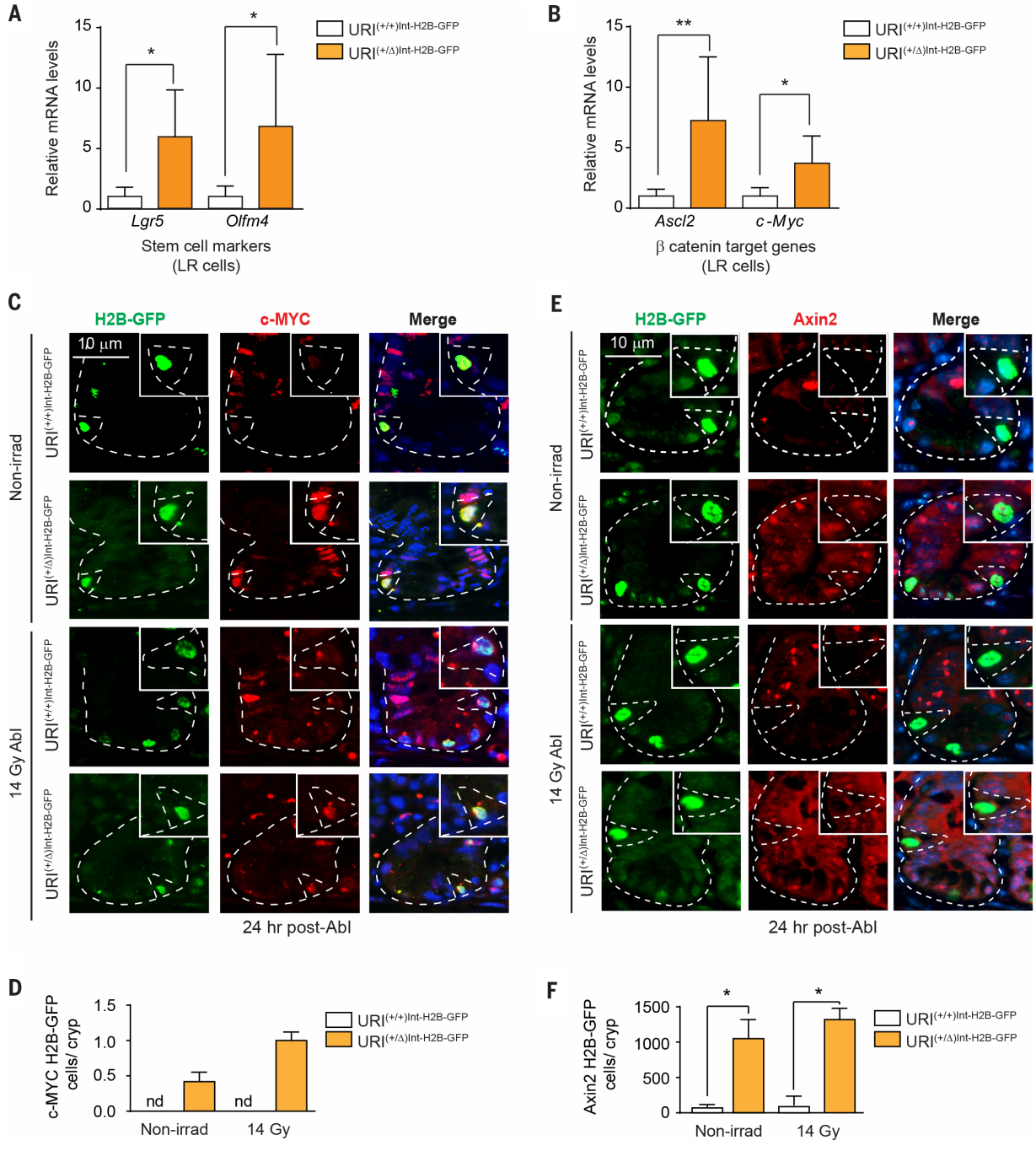

Fig. 5. URI loss activates β-catenin–c-MYC axis in LR cells. (**A** and **B**) qRT-PCR of *Lgr5* and *Olfm4* (A) and *Ascl2* and *c-Myc* (B) mRNA levels in LR cells sorted from URI$^{Int\text{-}H2B\text{-}GFP}$ mice after 15 days of tamoxifen treatment (n = 3 per group). (**C** and **D**) Co-IF (C) and quantification (D) of H2B-GFP and c-MYC in intestinal sections from nonirradiated and 14-Gy–abdominally irradiated URI$^{Int\text{-}H2B\text{-}GFP}$ mice after 15 days of tamoxifen treatment. Insets in (C) are magnified views. nd, not detected. (**E** and **F**) Co-IF (E) and quantification (F) of H2B-GFP and Axin2 in intestinal sections from nonirradiated and 14-Gy–abdominally irradiated URI$^{Int\text{-}H2B\text{-}GFP}$ mice after 15 days of tamoxifen treatment. Insets in (E) are magnified views. Data represent mean ± SEM. In (A), (B), (D), and (F), *P < 0.05 and **P < 0.01 by Student's t test analysis. Quantification was performed over 50 crypts per mouse in three independent mice. Dashed white lines represent crypts in nonirradiated mice and RAs in 14-Gy-abdominally irradiated mice.

and cell number (figs. S11D and S23, E and F). Additionally, in HCT-116 cells, URI down-regulation (using *URI*-silencing RNA) increased Axin 2 and c-MYC expression, whereas HA (hemagglutinin)–URI overexpression reduced their levels (fig. S23, G to J). Thus, URI loss activates WNT–β-catenin signaling pathway in TA-LR cells. Accordingly, URI overexpression in Lgr5^{high} ISCs [hURI$^{(+/KI)Int\text{-}Lgr5\text{-}EGFP}$] decreased expression of WNT–β-catenin target genes and stemness (fig. S23, K and L) without affecting numbers of cells per crypt (fig. S23M).

URI binds and inhibits β-catenin nuclear translocation

Cytosolic biochemical fractionation of HCT-116 cells and crypts isolated from URI$^{(+/+)Int}$ and URI$^{(\Delta/\Delta)Int}$ mice after 6 days of tamoxifen treatment demonstrated that URI depletion

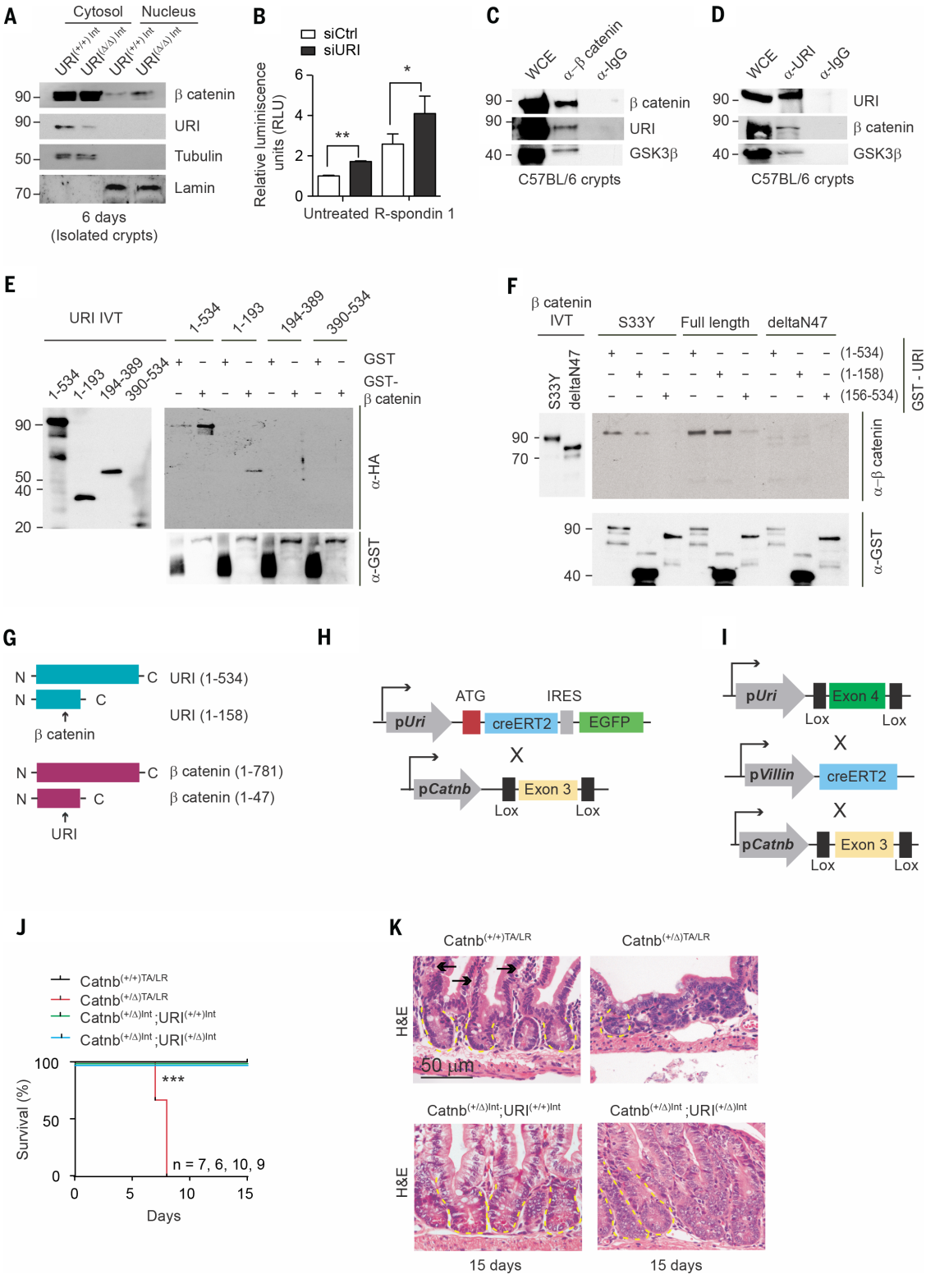

Fig. 6. URI binds and inhibits β-catenin nuclear translocation. (**A**) WB of nuclear and cytosolic fractions of crypts from URI$^{Int\text{-}H2B\text{-}GFP}$ mice after 6 days of tamoxifen treatment. Numbers to the left of the blot are in kDa. Tubulin and lamin were used as loading controls. (**B**) TOP-FOP reporter assay in HCT-116 cells 48 hours after transfection with either small interfering RNA (siRNA) control (siCtrl) or siRNA against *URI* (siURI) and treated with or without R-spondin 1 (n = 3). RLU, relative luminescence units. (**C** and **D**) β-catenin (C) and URI (D) immunoprecipitation in crypts from C57BL/6 mice. WCE, whole-cell extract; IgG, immunoglobulin G. Numbers to the left of the blots are in kDa. (**E**) Pull-down of IVT full-length HA-URI (residues 1 to 534) and HA-URI fragments (residue ranges indicated) using GST or GST–β-catenin. Numbers to the left of the blots are in kDa. (**F**) Pull-down of IVT full-length β-catenin (residues 1 to 781), β-catenin mutants (S33Y) and (deltaN47) using full-length GST-URI (residues 1 to 534) or GST-URI fragments (residues 1 to 158 and 156 to 534). Numbers to the left of the blots are in kDa. (**G**) Schematic showing β-catenin binding to URI and vice versa. N, N terminus; C, C terminus. (**H** and **I**) Schematics showing the cross between the URI-creERT2-IRES-EGFP mouse and the *Catnb*$^{+/lox(ex3)}$ mouse (H) and between the URI lox; Villin-creERT2 mouse and the *Catnb*$^{+/lox(ex3)}$ mouse (I). (**J**) Kaplan-Meier curve of Catnb$^{(+/+)TA/LR}$ mice, Catnb$^{(+/\Delta)TA/LR}$ mice, Catnb$^{(+/\Delta)Int}$;URI$^{(+/+)Int}$ mice, and Catnb$^{(+/\Delta)Int}$;URI$^{(+/\Delta)Int}$ mice. (**K**) H&E staining from Catnb$^{(+/+)TA/LR}$, Catnb$^{(+/\Delta)TA/LR}$, Catnb$^{(+/\Delta)Int}$;URI$^{(+/+)Int}$, and Catnb$^{(+/\Delta)Int}$;URI$^{(+/\Delta)Int}$ mice at indicated time points of tamoxifen treatment. Yellow dashed lines and black arrows represent crypt and villi, respectively. Data represent mean ± SEM. In (B) and (J), *P < 0.05, **P < 0.01, and ***P < 0.001 by Student's t test analysis (B) and Mantel-Cox test analysis (J).

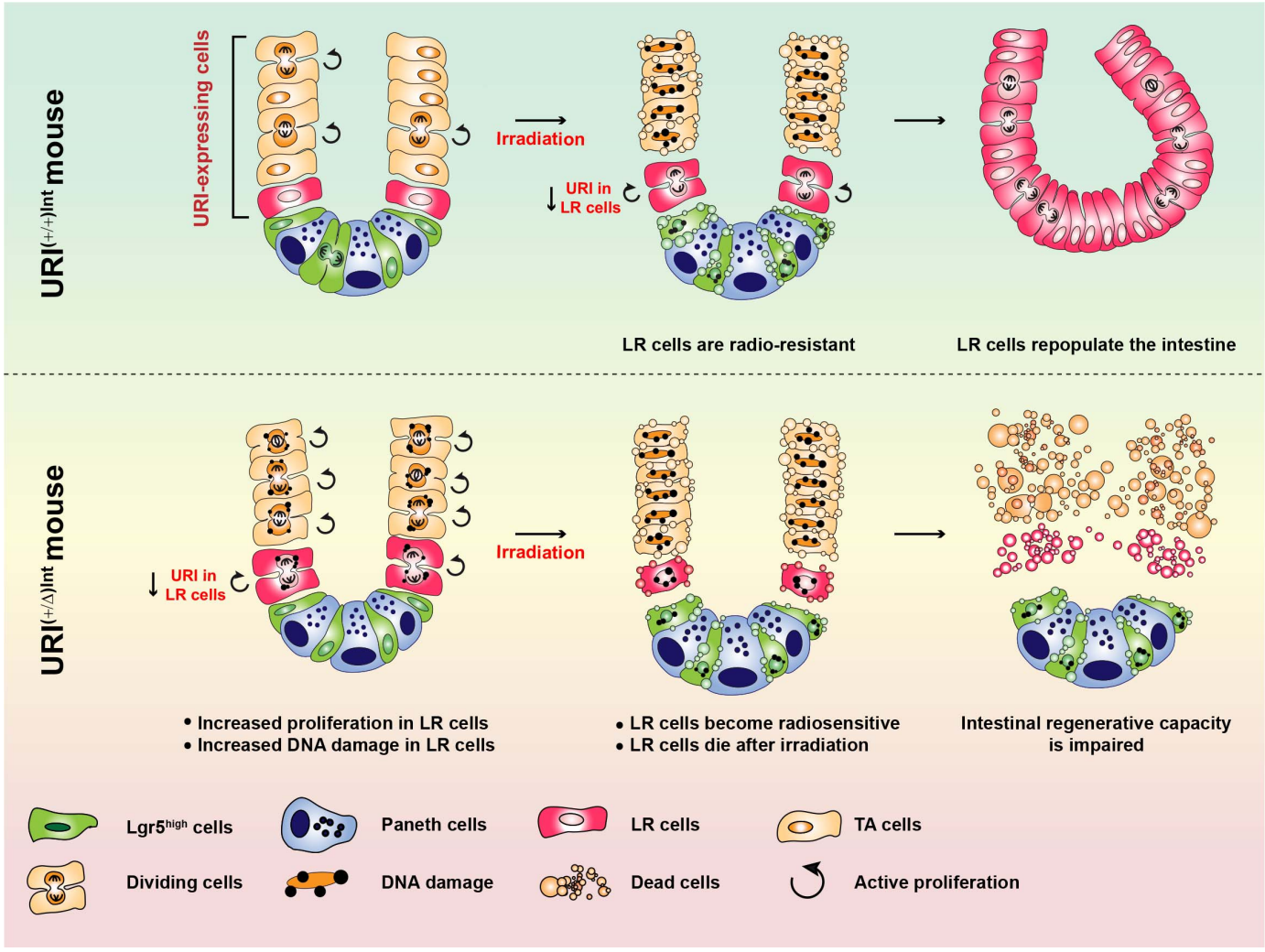

Fig. 7. Mechanisms of GIS. Schematics depicting the mechanisms of GIS after URI deletion in intestinal epithelium.

increased nuclear localization of β-catenin (Fig. 6A and fig. S24A). Notably, β-catenin stability was not affected in URI$^{(\Delta/\Delta)Int}$ crypts (fig. S24B). TOP-FOP reporter assays of β-catenin transcriptional activity in HCT-116 cells demonstrated that URI down-regulation increased luciferase activity, whereas overexpression of HA-URI diminished it (Fig. 6B and fig. S24C). Thus, URI loss in TA-LR cells may selectively activate the canonical WNT–β-catenin pathway, possibly inducing TA-LR cell proliferation and stemness.

URI is part of a complex that inhibits several enzymes and transcription factors (*18*, *22*, *23*). We thus checked whether URI inhibits β-catenin activity by means of direct physical interaction that abolishes its nuclear translocation. In reciprocal immunoprecipitation assays, endogenous URI and β-catenin interacted in C57BL/6 crypts and HCT-116 cells (Fig. 6, C and D, and fig. S24, D and E). We therefore evaluated the direct binding of URI and β-catenin in vitro by incubating recombinant glutathione *S*-transferase (GST) or GST-tagged β-catenin with in vitro translated (IVT) full-length HA-URI or selected HA-URI fragments. Pull-down assays revealed that URI's prefoldin N-terminal (Nt) domain (residues 1 to 193) interacted with β-catenin (Fig. 6E). This interaction was verified by incubating GST-URI or GST-URI fragments with IVT full-length β-catenin or various Flag-tagged β-catenin mutants. Full-length β-catenin bound to URI's Nt prefoldin domain (residues 1 to 158) (fig. S24, F to H). An Nt-truncated β-catenin mutant (deltaN47) with high T cell factor (TCF) activity did not interact with URI. Additionally, URI bound less strongly to the β-catenin mutant S33Y (Ser^{33}→Tyr), which exhibits enhanced β-catenin activity (Fig. 6F and fig. S24, I and J). Thus, β-catenin binds to URI's Nt and vice versa (Fig. 6G), suggesting that direct binding to URI inhibits the nuclear translocation of β-catenin.

To check whether β-catenin activation in TA-LR cells disrupts intestinal architecture, recapitulating features of URI$^{(\Delta/\Delta)Int}$ mice and GIS, we crossed URI-creERT2-IRES-EGFP mice with a conditional β-catenin–targeted mouse strain, *Catnb*$^{+/lox(ex3)}$, generating Catnb$^{(+/\Delta)TA/LR}$ mice with constitutive activation of β-catenin in TA-LR cells, owing to the absence of glycogen synthase kinase 3 (GSK3) phosphorylation sites in β-catenin's Nt domain and URI binding site after tamoxifen treatment (Fig. 6H). Catnb$^{(+/\Delta)TA/LR}$ mice died after 8 days of tamoxifen treatment, and Catnb$^{(+/\Delta)TA/LR}$ intestines showed crypt hypoplasia with evidence of DNA damage, fibrosis, and reduced numbers of villi (Fig. 6, J and K, and fig. S24K), recapitulating features of URI$^{(\Delta/\Delta)Int}$ mice. Mice expressing activated β-catenin throughout their intestines, obtained by crossing *Catnb*$^{+/lox(ex3)}$ and Villin-creERT2 mice [Catn$^{(+/\Delta)Int}$], survived and exhibited mild crypt hyperplasia, but no defects in intestinal structure, after 15 days of tamoxifen treatment, possibly because of β-catenin overactivation in the mitotically active Lgr5^{high} ISCs (Fig. 6, I to K). Shortened villi with loss of absorptive enterocytes and more pronounced crypt hyperplasia were detected in Catn$^{(+/\Delta)Int}$;URI$^{(+/\Delta)Int}$ mice [generated by crossing Catn$^{(+/lox)Int}$ and URI lox mice] after 15 days of tamoxifen treatment (Fig. 6, I to K). The presence of URI thus modulates compartment-dependent differential activation of β-catenin, leading to different phenotypes.

Discussion

We show here that URI labels quiescent LR cells to maintain their identity and organ architecture during IR. Halving URI expression renders LR cells highly proliferative, and hence radiosensitive (Fig. 7), whereas complete URI reductions induce LR cell death and impairment of intestinal regenerative capacity. In line with these findings, URI overexpression in mice [hURI$^{(+/KI)Int}$ mice] protects LR cells from lethal irradiation doses, allowing a better regenerative capacity after intense irradiation. Although URI^{+} LR cells survive IR in hURI$^{(+/KI)Int}$ mice, they should also proliferate to allow organ regeneration. URI levels in RAs of irradiated hURI$^{(+/KI)Int}$ mice were similar to URI levels in RAs of hURI$^{(+/+)Int}$ mice (not shown). Thus, URI might be degraded by means of unknown mechanisms in hURI$^{(+/KI)Int}$ mice after IR, allowing active proliferation in RAs. We also do not exclude that IR-induced paracrine signals in hURI$^{(+/+)Int}$ mice can affect LR cell fate in irradiated hURI$^{(+/KI)Int}$ mice.

Our data argue that TA-LR cells in URI$^{(+/\Delta)Int}$ mice have stem cell–like traits, with high (potentially tumorigenic) DNA damage. URI binds less to the β-catenin mutants (deltaN47 and SY33), which are found in neoplastic intestinal lesions and which display high TCF activation (*24*), suggesting that URI loss may have a carcinogenic potential through β-catenin–c-MYC activation. It is also tempting to speculate that low URI expression in Lgr5^{high} ISCs may be responsible for these cells' high β-catenin activity and stemness. This is consistent with our findings demonstrating that URI overexpression in Lgr5^{high} ISCs reduces WNT–β-catenin signaling.

On the basis of our findings, we can speculate that selective inhibition of c-MYC may be a prime strategy for safeguarding intestinal tissue architecture during high-dose irradiation. c-MYC inhibitors may thus allow increases of radiation doses during cancer radiotherapy, decreasing off-target effects and, hence, providing a more effective way of treating tumors. Moreover, c-MYC inactivation may cause tumor shrinkage in these patients. Finally, further work is required to determine whether reduced URI levels could be valuable predictive indicators of patients' responses to high-dose irradiation.

Methods summary

To study the role of URI in radiation-induced GIS, conditional *Uri* knockout mice were generated by deletion of exon 4 of the *Uri* gene. URI was specifically ablated in intestinal epithelium by crossing conditional URI lox mice with Villin-creERT2 mice (*25*). Moreover, to study whether URI^{+} cells repopulate the intestine after high irradiation doses, URI knock-in mice were generated by inserting a creERT2-IRES-EGFP cassette under the control of the *Uri* promoter in exon 1 of the *Uri* gene and crossing with R26-stop-EYFP or URI-creERT2;CAG-Katushka mice.

To avoid bone marrow failure and specifically irradiate in the abdominal cavity, we designed a device using 3-cm lead chambers. Mice were anesthetized by using ketamine (100 mg/kg) and xylazine (10 mg/kg) and placed in a methacrylate chamber to hold them. Mice were fully protected except for a 3-cm open window where the abdominal cavity was located, allowing for absorption of 100% of the irradiation. The irradiator Mark I 30A system was used for irradiation of 8-week-old mice. The source used in this case was Cs-137 (662 KeV E.max). Doses ranging between 2 and 22 Gy were delivered at a dose rate of 1.54 Gy/min, and mice were sacrificed at different time points.

REFERENCES AND NOTES

1. F. A. Mettler Jr., G. L. Voelz, Major radiation exposure—What to expect and how to respond. *N. Engl. J. Med.* **346**, 1554–1561 (2002). doi: 10.1056/NEJMra000365; pmid: 12015396
2. J. M. Novak *et al*., Effects of radiation on the human gastrointestinal tract. *J. Clin. Gastroenterol.* **1**, 9–40 (1979). doi: 10.1097/00004836-197903000-00003; pmid: 400660
3. N. Barker *et al*., Identification of stem cells in small intestine and colon by marker gene *Lgr5*. *Nature* **449**, 1003–1007 (2007). doi: 10.1038/nature06196; pmid: 17934449
4. H. Clevers, The intestinal crypt, a prototype stem cell compartment. *Cell* **154**, 274–284 (2013). doi: 10.1016/j.cell.2013.07.004; pmid: 23870119
5. J. Beumer, H. Clevers, Regulation and plasticity of intestinal stem cells during homeostasis and regeneration. *Development* **143**, 3639–3649 (2016). doi: 10.1242/dev.133132; pmid: 27802133
6. S. J. Buczacki *et al*., Intestinal label-retaining cells are secretory precursors expressing Lgr5. *Nature* **495**, 65–69 (2013). doi: 10.1038/nature11965; pmid: 23446353
7. G. Hua *et al*., Crypt base columnar stem cells in small intestines of mice are radioresistant. *Gastroenterology* **143**, 1266–1276 (2012). doi: 10.1053/j.gastro.2012.07.106; pmid: 22841781
8. C. Metcalfe, N. M. Kljavin, R. Ybarra, F. J. de Sauvage, *Lgr5*$^{+}$ stem cells are indispensable for radiation-induced intestinal regeneration. *Cell Stem Cell* **14**, 149–159 (2014). doi: 10.1016/j.stem.2013.11.008; pmid: 24332836
9. W. J. Zhou, Z. H. Geng, J. R. Spence, J. G. Geng, Induction of intestinal stem cells by R-spondin 1 and Slit2 augments chemoradioprotection. *Nature* **501**, 107–111 (2013). doi: 10.1038/nature12416; pmid: 23903657
10. C. S. Xu *et al*., MSP58 knockdown inhibits the proliferation of esophageal squamous cell carcinoma in vitro and in vivo. *Asian Pac. J. Cancer Prev.* **13**, 3233–3238 (2012). doi: 10.7314/APJCP.2012.13.7.3233; pmid: 22994740
11. R. K. Montgomery *et al*., Mouse telomerase reverse transcriptase (mTert) expression marks slowly cycling intestinal stem cells. *Proc. Natl. Acad. Sci. U.S.A.* **108**, 179–184 (2011). doi: 10.1073/pnas.1013004108; pmid: 21173232
12. A. E. Powell *et al*., The pan-ErbB negative regulator Lrig1 is an intestinal stem cell marker that functions as a tumor suppressor. *Cell* **149**, 146–158 (2012). doi: 10.1016/j.cell.2012.02.042; pmid: 22464327
13. W. Qiu *et al*., PUMA regulates intestinal progenitor cell radiosensitivity and gastrointestinal syndrome. *Cell Stem Cell* **2**, 576–583 (2008). doi: 10.1016/j.stem.2008.03.009; pmid: 18522850
14. K. S. Yan *et al*., The intestinal stem cell markers Bmi1 and Lgr5 identify two functionally distinct populations. *Proc. Natl. Acad. Sci. U.S.A.* **109**, 466–471 (2012). doi: 10.1073/pnas.1118857109; pmid: 22190486
15. P. Fei, W. S. El-Deiry, P53 and radiation responses. *Oncogene* **22**, 5774–5783 (2003). doi: 10.1038/sj.onc.1206677; pmid: 12947385
16. D. G. Kirsch *et al*., p53 controls radiation-induced gastrointestinal syndrome in mice independent of apoptosis. *Science* **327**, 593–596 (2010). doi: 10.1126/science.1166202; pmid: 20019247
17. B. Hu *et al*., The DNA-sensing AIM2 inflammasome controls radiation-induced cell death and tissue injury. *Science* **354**, 765–768 (2016). doi: 10.1126/science.aaf7532; pmid: 27846608
18. K. S. Tummala *et al*., Inhibition of de novo NAD^{+} synthesis by oncogenic URI causes liver tumorigenesis through DNA damage. *Cancer Cell* **26**, 826–839 (2014). doi: 10.1016/j.ccell.2014.10.002; pmid: 25453901
19. C. T. Parusel, E. A. Kritikou, M. O. Hengartner, W. Krek, M. Gotta, URI-1 is required for DNA stability in *C. elegans*. *Development* **133**, 621–629 (2006). doi: 10.1242/dev.02235; pmid: 16436622
20. K. A. Lipinski *et al*., Colorectal cancer cells display chaperone dependency for the unconventional prefoldin URI1. *Oncotarget* **7**, 29635–29647 (2016). doi: 10.18632/oncotarget.8816; pmid: 27105489
21. Z. Mao, A. Seluanov, Y. Jiang, V. Gorbunova, TRF2 is required for repair of nontelomeric DNA double-strand breaks by homologous recombination. *Proc. Natl. Acad. Sci. U.S.A.* **104**, 13068–13073 (2007). doi: 10.1073/pnas.0702410104; pmid: 17670947
22. S. Burén *et al*., Regulation of OGT by URI in response to glucose confers c-MYC-dependent survival mechanisms. *Cancer Cell* **30**, 290–307 (2016). doi: 10.1016/j.ccell.2016.06.023; pmid: 27505673
23. N. Djouder *et al*., S6K1-mediated disassembly of mitochondrial URI/PP1γ complexes activates a negative feedback program that counters S6K1 survival signaling. *Mol. Cell* **28**, 28–40 (2007). doi: 10.1016/j.molcel.2007.08.010; pmid: 17936702
24. F. T. Kolligs, G. Hu, C. V. Dang, E. R. Fearon, Neoplastic transformation of RK3E by mutant β-catenin requires deregulation of Tcf/Lef transcription but not activation of *c-myc* expression. *Mol. Cell. Biol.* **19**, 5696–5706 (1999). doi: 10.1128/mcb.19.8.5696; pmid: 10409758
25. F. El Marjou *et al*., Tissue-specific and inducible Cre-mediated recombination in the gut epithelium. *Genesis* **39**, 186–193 (2004). doi: 10.1002/gene.20042; pmid: 15282745

ACKNOWLEDGMENTS

We are very thankful to all the mouse providers as described in materials and methods. We also thank the CNIO Transgenic Mice Core Unit for technical support. **Funding:** A.C.-P. is a recipient of the La Caixa Ph.D. fellowship. N.D. is a recipient of the Spanish Ramón y Cajal fellowship. This work was supported by the Spanish Ministry of Economy and Competitiveness and co-funded by the European Regional Development Fund (ERDF-EU, SAF2016-76598-R) and the National Institute of Health Carlos III. **Author contributions:** A.C.-P. designed and performed most of the experiments. A.C.-P. and N.D. generated the URI-creERT2-IRES-EGFP mouse. M.Y. initiated the project, designed experiments, and engineered the URI lox allele with N.D. C.P. performed all histopathological analyses of murine tissues. S.d.l.R. characterized the URI-creERT2-IRES-EGFP mouse and helped with studying NHEJ repair in vitro. All authors analyzed the data. N.D. designed the experiments and conceived, developed, and wrote the project and study. N.D. wrote the manuscript and secured all funding. **Competing interests:** The authors declare no competing financial interests. **Data and materials availability:** All data are available in the main text or the supplementary materials. Materials are available upon request to N.D., and the sharing of materials described in this work will be subject to standard material transfer agreements.

SUPPLEMENTARY MATERIALS

science.sciencemag.org/content/364/6443/eaaq1165/suppl/DC1
Materials and Methods
Figs. S1 to S24
Tables S1 to S4
References (*26*–*37*)
Movie S1

4 October 2017; resubmitted 13 August 2018
Accepted 10 April 2019
10.1126/science.aaq1165